Convective Heat Transfer within Fibrous Insulation Slabs

D. K. Joshi and S. P. Sukhatme, Bombay (India)

Abstract. A numerical study of convective heat flow within a fibrous insulating slab is presented. The material is treated as an anisotropic porous medium and the variation of properties with temperature is taken into account. Good agreement is obtained with available experimental data for the same geometry.

Zusammenfassung. Für den konvektiven Wärmestrom in einem faserförmigen Isolierstoff wird eine numerische Berechnung angegeben. Der Stoff wird als anisotropes poröses Medium mit temperaturabhängigen Stoffwerten angesehen. Die Übereinstimmung mit verfügbaren Versuchswerten ist gut.

Nomenclature

C_p specific heat of the gas at the mean temperature

Da Darcy number $= k_y/H^2$

Gr^* modified Grashof number $= g\beta\Delta T H k_y/\nu^2$
       $=$ (Grashof number) x (Darcy number)

H thickness of the specimen

P gas pressure

Pr^* modified Prandtl number $= \mu C_p/\lambda_x$

Ra^* modified Rayleigh number $= Gr^* Pr^*$

R_p ratio of permeabilities $= k_y/k_x$

R_k ratio of conductivities $= \lambda_y/\lambda_x$

T absolute temperature of the gas

T_1 absolute temperature of the hot face

T_2 absolute temperature of the cold face

T_m mean temperature of the gas $= (T_1 + T_2)/2$

k_x specific permeability of the porous medium along the x-direction

k_y specific permeability of the porous medium along the y-direction

p $\Delta T/T_m$

q exponent

r exponent

u gas velocity along the x-direction

v gas velocity along the y-direction

x_* distance along the x-direction

y_* distance along the y-direction

ΔT temperature difference $= T_1 - T_2$

β thermal coefficient of expansion of the gas

β_m thermal coefficient of expansion of the gas at the mean temperature

θ^* $T - T_m$

θ dimensionless temperature $= \theta^*/\Delta T$

λ_a apparent thermal conductivity of the porous medium along the x-direction

λ_{al} local apparent thermal conductivity of the porous medium along the x-direction

λ_x thermal conductivity of the porous medium along the x-direction in the absence of convection

λ_y thermal conductivity of the porous medium along the y-direction in the absence of convection

μ dynamic viscosity of the gas

μ_m dynamic viscosity of the gas at the mean temperature

ν kinematic viscosity of the gas

ν_m kinematic viscosity of the gas at the mean temperature

ρ density of the gas

ρ_m density of the gas at the mean temperature

ψ^* stream function at any point

ψ dimensionless stream function $= \psi^*/(\mu_m/\rho_m)$

1. Introduction

Like many other insulations, fibrous insulating materials owe their insulating value to the low thermal conductivity of air. The heat flow through such materials consists of the following contributions:

i) Convective heat transfer through the air
ii) Radiation heat transfer
iii) Conduction heat transfer through the solid fibres.

The effectiveness of the insulations lies in their ability to suppress the contribution due to convective heat transfer to the maximum extent possible, while at the same time minimizing the contributions due to radiation and solid conduction.

This paper is concerned with calculating the first contribution. The problem of calculating the other two contributions has been extensively dealt with elsewhere, e. g. references [1] to [10].

2. Literature Review

2.1 Analytical Work

Lotz [11] has presented an approximate analysis for convective air flow in vertical glass wool bats with either or both of the vertical faces permeable. The approximations include the assumptions that a certain flow pattern exists and that a linear temperature distribution exists within the slab inspite of the convective heat flow. In a similar manner, Wolf [12] has analyzed a porous partition permitting convective air flow from the hot to the cold chambers. He has assumed that the flow is normal to the partition, that the temperature distribution within the partition is linear and that the temperatures in the hot and cold chambers are constant.

More sophisticated analyses are due to Chan et al. [13] and Elder [14] who have numerically solved the

energy and flow differential equations for vertical and horizontal isotropic porous slabs with impermeable boundaries. However, since these analyses are for isotropic media, they cannot be successfully used for predicting convection in fibrous insulation slabs, which are known to be highly anisotropic. Höglund [15] has reported that the ratio of resistance to flow in the two directions of a fibrous insulation slab could be of the order of two. Analysis of convection in an anisotropic porous medium is therefore undertaken in this paper.

2.2. Experimental Investigations

Several research workers [11, 16–26] have reported experimental results about convective heat transfer in horizontal and vertical insulation slabs. Griffiths [21] reported a 50 per cent increase in conductivity for a 60 inches high and 6 inches thick glass fibre mat of density 12 lb/ft^3 subjected to a horizontal temperature gradient of 50 °F/inch. His results indicated that convective heat transfer increased with the L/H ratio. Allcut and Ewens [17] tested rock-wool samples in a horizontal position with a temperature difference of about 33 °F. A 30 per cent increase in conductivity was reported with an increase in thickness from 1 to 4$^1/_2$ inch. Allcut [16] tested various insulating materials at different air pressures. The difference between the variation of conductivity (in the absence of radiation) of the insulating material with pressure and the variation of conductivity of air with pressure was attributed to convection. This was reported to be 0.04–0.02 (Btu-inch/ft^2-°F-hour) for 1.25–3.2 lb/ft^3 density glass wool, i. e. 10–14 per cent of the corresponding values of apparent conductivity reported. Cammerer [20] reported results of tests on 20–100 kg/m^3 density glass wool panels of up to 1.5 metres height and thicknesses of 50, 100 and 200 mm. A considerable variation of temperature along the height of the panels was measured indicating the presence of convection currents. However it was pointed out that the differences in conductivities for different panel heights and thicknesses were of the order of 6 per cent, whereas the accuracy of measurement of the conductivity was ± 5 per cent. The local apparent thermal conductivity as measured at the hot face by a heat flow meter was found to be considerably higher near the bottom in comparison with a corresponding value nearer the top.

Zehendner [26] conducted careful tests on superfine glass wool bats of 8 kg/m^3 density at low temperatures. Data was presented for a specimen of size 200 x 200 x 40 mm. The specimen was tested horizontally with heat flow downwards and upwards and vertically with heat flow sideways. The difference in heat flow between the cases of heat flow upwards or sideways and the case of downwards heat flow at any particular temperature gradient was ascribed to convection. The convection contribution was found to be

inversely proportional to the fourth power of absolute temperature and to be significant at temperatures below − 50 °C. A maximum value of $(\lambda_a/\lambda_x) = 1.75$ for a specimen mean temperature of − 150 °C and a horizontal temperature gradient of 20 °C/cm was obtained. Kostelyne [23] conducted tests in a cylindrical apparatus and observed convection only with fibre diameters greater than 19 μ. Lotz [11] carried out investigations in cold storages and observed that for fibre glass insulation in the density range of 48 to 64 kg/m^3, the contribution due to convection was very small. Wolf [25] obtained the temperature variation along the height of glass wool bats with both closed and open faces.

Baker [18] presented data about the effect of pressure on the convective contribution.

3. Analysis

The analysis is conducted for a slab of height L and breadth H closed on all surfaces (Fig. 1). The two vertical faces are maintained at constant temperatures T$_1$ and T$_2$, while the horizontal faces are assumed to be insulated. Some results have also been obtained by assuming the temperature distribution along these boundaries to be linear.

As is usual for porous media, Darcy's law is assumed to be valid. Viscous drag and inertia terms are neglected as their contribution is likely to be negligible. Since the ratio of the temperature difference across the slab and the mean temperature is high in many cases, the variation of μ, ρ and β with temperature is taken into account. The properties k_x, k_y and C_p are however assumed constant. This is a reasonable assumption. The governing equations of continuity, flow and energy may then be written down as follows:

$$\frac{\partial}{\partial x_*} (\rho u) + \frac{\partial}{\partial y_*} (\rho v) = 0 , \qquad (1)$$
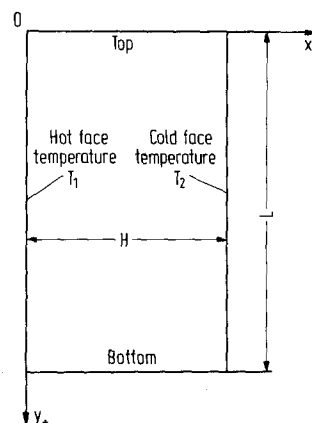

Fig. 1. Configuration under study

$$\frac{\mu}{k_x} u = -\frac{\partial P}{\partial x_*},$$ (2)

$$\frac{\mu}{k_y} v = -\frac{\partial P}{\partial y_*} - g\beta\rho(T - T_m),$$ (3)

$$C_p \left[\rho u \frac{\partial \theta^*}{\partial x_*} + \rho v \frac{\partial \theta^*}{\partial y_*}\right]$$

$$= \lambda_x \frac{\partial^2 \theta^*}{\partial x_*^2} + \frac{\partial \theta^*}{\partial x_*}\frac{\partial \lambda_x}{\partial x_*} + \lambda_y \frac{\partial^2 \theta^*}{\partial y_*^2} + \frac{\partial \theta^*}{\partial y_*}\frac{\partial \lambda_y}{\partial y_*}.$$ (4)

Eliminating P from Eqs. (2) and (3) and defining stream function ψ^* as

$$\rho u = \frac{\partial \psi^*}{\partial y_*} \quad \text{and} \quad \rho v = -\frac{\partial \psi^*}{\partial x_*}$$

the following equations are obtained

$$\frac{1}{k_x}\frac{\partial}{\partial y_*}\left(\nu \frac{\partial \psi^*}{\partial y_*}\right) + \frac{1}{k_y}\frac{\partial}{\partial x_*}\left(\nu \frac{\partial \psi^*}{\partial x_*}\right) = g\frac{\partial}{\partial x_*}(\rho\beta\theta^*),$$ (5)

$$\frac{\partial \psi^*}{\partial y_*}\frac{\partial \theta^*}{\partial x_*} - \frac{\partial \psi^*}{\partial x_*}\frac{\partial \theta^*}{\partial y_*} =$$

$$\frac{1}{C_p}\left[\lambda_x \frac{\partial^2 \theta^*}{\partial x_*^2} + \frac{\partial \lambda_x}{\partial \theta^*}\left(\frac{\partial \theta^*}{\partial x_*}\right)^2 + \lambda_y \frac{\partial^2 \theta^*}{\partial y_*^2} + \frac{\partial \lambda_y}{\partial \theta^*}\left(\frac{\partial \theta^*}{\partial y_*}\right)^2\right].$$ (6)

The boundary conditions are:

$$x_* = 0, \quad \psi^* = 0, \quad \theta^* = T_1 - T_m = \frac{\Delta T}{2},$$

$$x_* = H, \quad \psi^* = 0, \quad \theta^* = T_2 - T_m = -\frac{\Delta T}{2}$$

and for $y_* = 0$ and $y_* = L$

$$\psi^* = 0 \quad \text{and either} \quad \frac{\partial \theta^*}{\partial y_*} = 0 \quad \text{or}$$

$$\frac{\partial \theta^*}{\partial x_*} = \text{constant} = -\frac{\Delta T}{H}.$$

The temperature, stream function and length are made dimensionless by dividing the quantities by ΔT, μ_m and H respectively. The variation of the properties ρ, β, and ν for air with temperature can be expressed in exponential form to a fair degree of accuracy. We therefore assume the following functional relationships.

$$\rho\beta = \rho_m\beta_m \left(\frac{T_m}{T}\right)^q \quad \text{and} \quad \nu = \nu_m \left(\frac{T}{T_m}\right)^r.$$

Further, introducing $p = \frac{\Delta T}{T_m}$ we get $\frac{T}{T_m} = 1 + p\theta$.

Eq. (5) can thus be rewritten as

$$R_p \frac{\partial^2 \psi}{\partial y^2} + \frac{\partial^2 \psi}{\partial x^2} + \frac{rp}{1+p\theta}\left(R_p \frac{\partial \psi}{\partial y}\frac{\partial \theta}{\partial y} + \frac{\partial \psi}{\partial x}\frac{\partial \theta}{\partial x}\right)$$

$$= Gr^*\left[\frac{1-(q-1)p\theta}{(1+p\theta)^{q+r+1}}\right]\frac{\partial \theta}{\partial x}.$$ (7)

The solution of this equation is to be compared with Zehendner's [26] data. The maximum value of p in that data works out to be 0.65. For this value of p the expression

$$\frac{1-(q-1)p\theta}{(1+p\theta)^{q+r+1}} Gr^*$$

which we may term as the local Grashof number, has a maximum value of 14.5 Gr* at the cold end and a minimum value of 0.1275 Gr* at the hot end provided q = r = 2. The corresponding variation of λ_x and λ_y is much lesser in magnitude and is therefore neglected. Thus Eq. (6) reduces to

$$Pr^*\left(\frac{\partial \psi}{\partial y}\frac{\partial \theta}{\partial x} - \frac{\partial \psi}{\partial x}\frac{\partial \theta}{\partial y}\right) = \frac{\partial^2 \theta}{\partial x^2} + R_k \frac{\partial^2 \theta}{\partial y^2}.$$ (8)

The corresponding boundary conditions are

x = 0,	$\theta = +0.5$,	$\psi = 0$
x = 1,	$\theta = -0.5$,	$\psi = 0$
y = 0,	$(\partial\theta/\partial y) = 0$ or $(\partial\theta/\partial x) = 1$,	$\psi = 0$
y = L/H,	$(\partial\theta/\partial y) = 0$ or $(\partial\theta/\partial x) = 1$,	$\psi = 0$.

The problem thus reduces to solving the coupled partial differential Eqs. (7) and (8) subject to the given boundary conditions.

Eq. (7) involves the dimensionless quantities p, q and r which decide the extent of variation of properties. With either p = 0 or q = r = 0, the problem reduces to the one of constant properties. The other dimensionless quantities are R_p and Gr*. R_p is the ratio of permeabilities and Gr* is a modified Grashof number, the product of the conventional Grashof number and the dimensionless permeability called the Darcy number. Higher values of Gr* correspond to higher stream function values. Eq. (8) involves the dimensionless quantities Pr* and R_k. Pr* is a modified Prandtl number while R_k is the ratio of conductivities. From the equations, one may infer that a higher value of Pr* would mean a higher convective contribution for the same stream function distribution. Considering this along with the earlier conclusion regarding the influence of Gr* we can expect Gr* Pr* (= Ra*) to determine the convective contribution to a large extent. A higher value of R_p will obviously result in lower values of the stream function.

4. Method of Solution

The differential equations have been solved by the finite difference method, the Peaceman and Rachford alternate line and row technique of scanning being used. Finite difference equations were written making use of a five point molecule for the stream function and for the temperature.

Initial guesses for the temperature and stream function were assumed on the basis of an approximate parameter perturbation solution of Eqs. (7) and (8), in which the value of p was taken to be zero. Substituting

$$\psi = \psi_0 + (Pr^*)\,\psi_1 + (Pr^*)^2\,\psi_2 + \ldots$$

$$\theta = \theta_0 + (Pr^*)\,\theta_1 + (Pr^*)^2\,\theta_2 + \ldots$$

in Eqs. (7) and (8) and solving, one gets

$$\theta_0 = \frac{1}{2} - x \,,$$

$$\theta_1 = -\frac{16\,Gr^*\,H}{\pi^5 L}\,x$$

$$\times \sum_{m=1,3,5}^{\infty} \sum_{n=1,3,5}^{\infty} \frac{\sin m\pi x \cos \dfrac{n\pi y}{L/H}}{m\left(m^2 + R_p n^2 \dfrac{H^2}{L^2}\right)\left(m^2 + n^2 \dfrac{H^2}{L^2}\right)}$$

and

$$\psi_0 = -\frac{16\,Gr^*}{\pi^4}\,x$$

$$\times \sum_{m=1,3,5}^{\infty} \sum_{n=1,3,5}^{\infty} \frac{1}{m\,n}\,\frac{\sin m\pi x \cos \dfrac{n\pi y}{L/H}}{m^2 + n^2 R_p \dfrac{H^2}{L^2}} \,.$$

Convergence for higher values of p was ensured by starting the solution with p = 0 and increasing it in small steps of 0.02.

5. Permeability Tests

In order to determine the range of values of Gr* and R_p for which the Eqs. (7) and (8) were to be solved, it was decided to measure the permeabilities of some available insulation bats. A simple apparatus was therefore constructed for the purpose. It consisted of a sheet metal ducting 15.5 cm in diameter, attached to the suction side of a blower. Samples were held in the ducting such that air flowed either along the fibre layers or across them. Provision was made for measurement of pressure drop across the insulation sample and the air flow rate. Air velocities were in the range of 5 to 40 cm/sec. The air temperature was varied from 20 to 100 °C and it was found to have no effect on the value of permeability. The results are presented in Table 1. It can be seen from Table 1 that whereas the values of the permeabilities depend strongly on both the fibre diameter and the density, the ratio of the two is more strongly influenced by the density than the fibre diameter.

6. Results and Discussion

On the basis of the results of the permeability tests, Eqs. (7) and (8) were solved for values of Ra* ranging from 5.6 to 179.2 in multiples of 2, R_p from 0.2 to 5 and (L/H) from 0.5 to 18. Values of R_k were chosen to be 0.8, 1.0 and 1.2. In all cases, finally the value of (λ_a/λ_x), which is a measure of the convection present, was obtained. The effect of variation of properties with temperature was studied for a specimen of (L/H) = 5, for values of p from 0 to 0.7 and values of Ra* up to 179.2 both for the linear temperature distribution as well as for the insulated boundary condition at the top and bottom. Other computations were done for the insulated boundary condition only and for p = 0. The effect of Prandtl number variation was studied and it was found that within the range of 0.5 and 0.35, the value of (λ_a/λ_x) depended on Ra* alone.

Table 1. Permeabilities of Some Insulation Samples

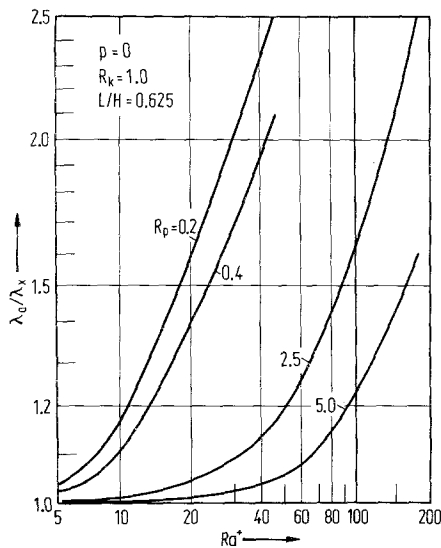| Description of bat	Density (kg/m³)	Permeability × 10⁵ (cm²)		Ratio Along layers / Across layers
		Across layers	Along layers	
Fine glass wool bat (Average fibre dia. < 2 μ)	10	0.2	0.45	2.25
Glass wool bat (Average fibre dia. 7 μ)	12	5.2	13.1	2.52
	16	3.6	8.5	2.36
	32	1.9	3.6	1.9
Mineral wool bat (Average fibre dia. 5 μ)	65	1.0	2.6	2.6

Fig. 2. Variation of (λ_a/λ_x) with Ra*, top and bottom boundaries insulated

The assumption that viscous drag and inertia force terms may be neglected was in fact verified by including them and solving a few cases for values of Da (which is the pertinent dimensionless parameter) ranging from 10^{-9} to 10^{-3}. It was found that for values of Da less than 10^{-4}, the effect of including these terms on the value of (λ_a/λ_x) was less than 0.5 per cent for L/H = 6, Gr* = 512, p = 0, Pr* = 0.35, R_p = 2.5 and R_k = 1.0. Since values of Da greater than 10^{-4} are rarely encountered, the assumption regarding viscous drag and inertia terms appears reasonable.

Fig. 2 shows the variation of (λ_a/λ_x) with Ra* for different values of R_p, (L/H) being constant and p = 0. It is seen that (λ_a/λ_x) rises quite slowly initially and then quite rapidly. The values of (λ_a/λ_x) for a particular value of Ra* and different values of R_p differ considerably at higher values of Ra*. Within the range of values of Ra* and (L/H) studied, no multi-cell formation is observed. This corresponds to what has been reported by Gill [27]. The stream function distribution shown for a particular case in Fig. 6 clarifies this point.

Fig. 3 shows the variation of (λ_a/λ_x) against (L/H) for different values of Ra* and R_p. It is seen that for particular values of Ra* and R_p, the value of (λ_a/λ_x) goes through a maximum. Further it is seen that for particular values of Ra*, the curves for different values of R_p tend to merge after the maximum as (L/H) increases. The behaviour observed in Fig. 3 agrees with the results reported by Cammerer [20] and indicates that the results of Griffiths [21] which have been obtained for large values of (L/H) are probably erroneous.

Fig. 3 also presents a comparison of the present results for R_p = 1 with the isotropic analysis of Chan et al. [13]. It will be noted that excellent agreement
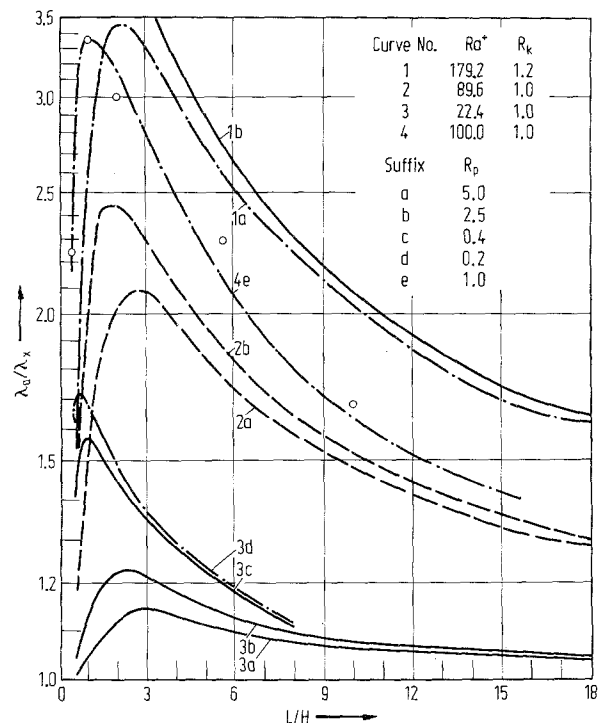

Fig. 3. Variation of (λ_a/λ_x) with (L/H) for insulated boundaries and p = 0.
0 represents points read from Chan et al.'s study

has been obtained, between curve 4e and the points read off from the calculations of reference [13].

Fig. 4 shows the effect of considering the variation of properties. The variation of (λ_a/λ_x) with Ra* for different values of p with both the boundary conditions is plotted. It is seen that the linear temperature boundary condition results in unequal heat flows at the hot and cold faces, for non-zero values of p, the heat flow at the hot face being lower than that at the cold face. It is also seen that the linear temperature boundary condition results in considerably smaller values of (λ_a/λ_x) at both the vertical faces as compared with the values for the insulated boundary condition. These points are further elaborated in Fig. 5, which shows the variation of (λ_a/λ_x) with p for the two boundary conditions at fixed values of Ra*.

Figs. 6 and 7 show details of the solution obtained in a particular case (viz. Ra* = 179.2, L/H = 6, p = 0, R_k = 1, R_p = 2.5) with the insulated boundary condition. Fig. 6 shows the stream function distribution, while Fig. 7 shows the variation of temperature close to the hot face and of (λ_{a1}/λ_x) along the hot face.

The stream function distribution can be seen to be symmetric about either of the diagonals so that $\psi(x, y) = \psi(1 - x, L/H - y)$. This corresponds to what has been pointed out by Rubel [28]. This symmetry in distribution of stream function as well as the antisymmetry in the distribution of temperature,
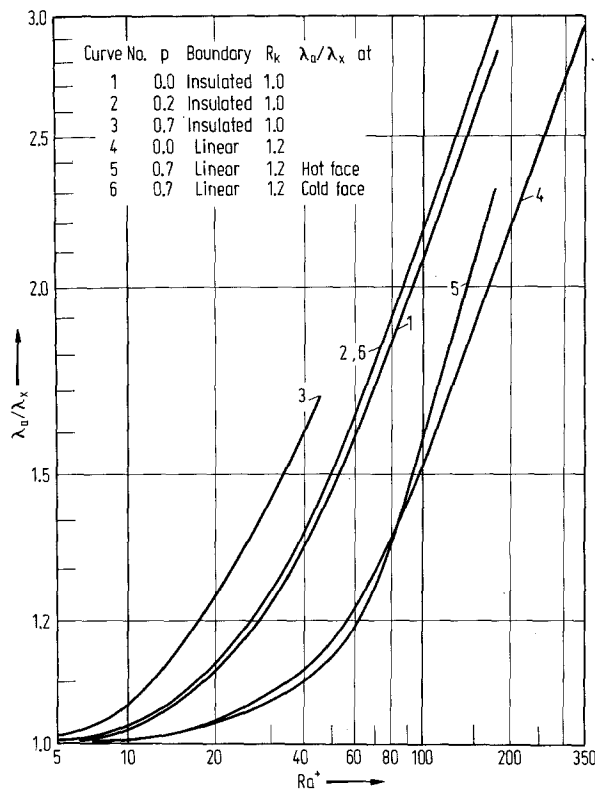
Curve No.	p	Boundary	R_k	λ_a/λ_x at
1	0.0	Insulated	1.0	
2	0.2	Insulated	1.0	
3	0.7	Insulated	1.0	
4	0.0	Linear	1.2	
5	0.7	Linear	1.2	Hot face
6	0.7	Linear	1.2	Cold face

Fig. 4. Variation of (λ_a/λ_x) with Ra* for different values of p. (L/H) = 5, R_p = 2.5
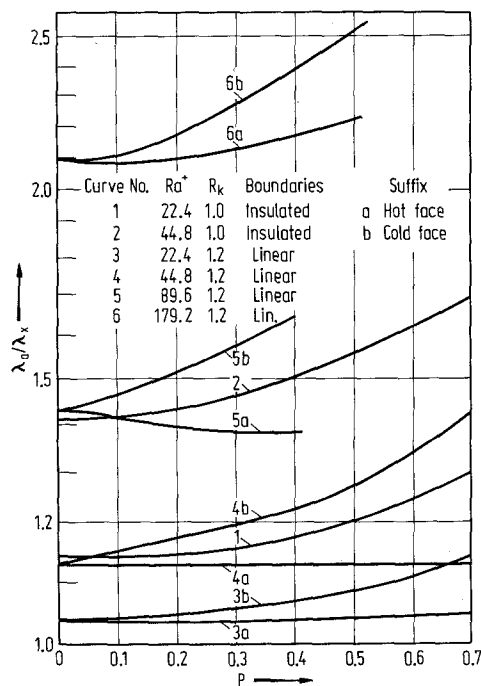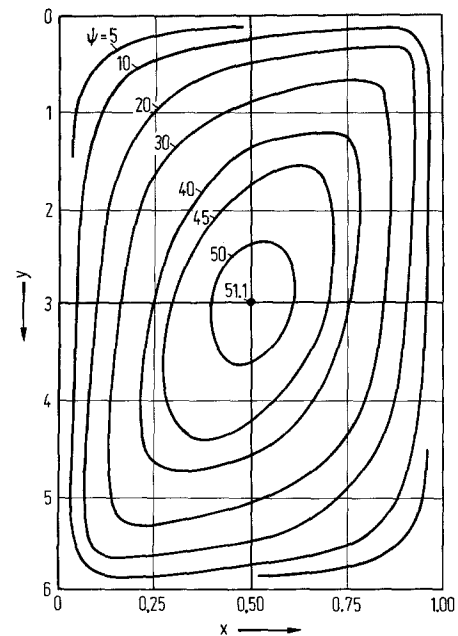

Fig. 6. Stream function distribution for Ra* = 179.2, (L/H) = 6, p = 0, R_k = 1, R_p = 2.5 with insulated boundary condition
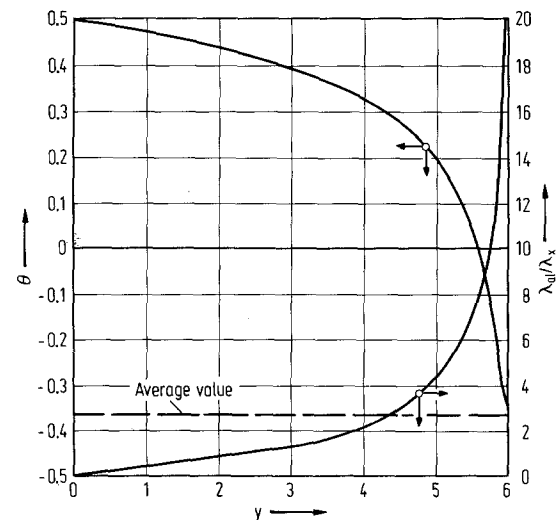

Curve No.	Ra*	R_k	Boundaries	Suffix
1	22.4	1.0	Insulated	a Hot face
2	44.8	1.0	Insulated	b Cold face
3	22.4	1.2	Linear	
4	44.8	1.2	Linear	
5	89.6	1.2	Linear	
6	179.2	1.2	Lin.	

Fig. 5. Variation of (λ_a/λ_x) with p for (L/H) = 5, R_p = 2.5

Fig. 7. Variation of temperature along y at x = (H/13) and of (λ_{a1}/λ_x) along y for Ra* = 179.2, (L/H) = 6, p = 0, R_k = 1, R_p = 2.5 with insulated boundary condition. Dotted line represents (λ_a/λ_x) for the same conditions.

viz. θ (x, y) = $- \theta$ (1 $-$ x, L/H $-$ y) was made use of in analysing the p = 0 case. The existence of such symmetry can be easily proved from the nature of the differential equations and the boundary conditions. Stream lines are also seen to be crowded near the bottom boundary of the hot face. At this point the upward buoyancy and therefore the upward velocity is a maximum. As a result, colder air rushes in resulting
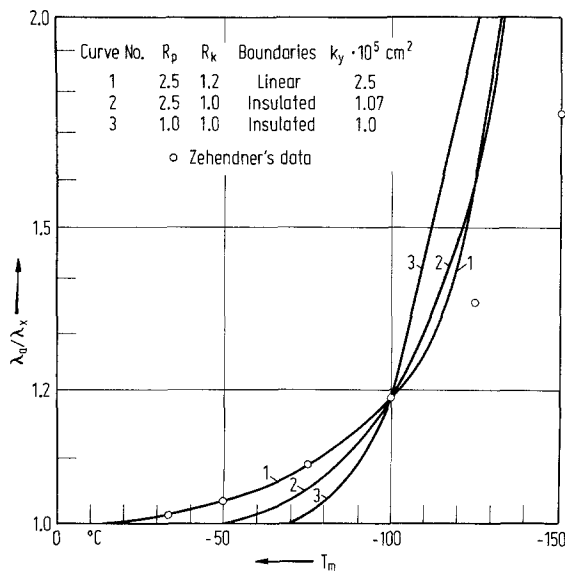
Fig. 8. Comparison of different solutions with Zehendner's data (indicated by circles) for a temperature difference of 80 °C. Curve numbers 1 and 2 represent variable property solutions. Curve 3 represents the constant property solution. Property values at mean temperature are used.
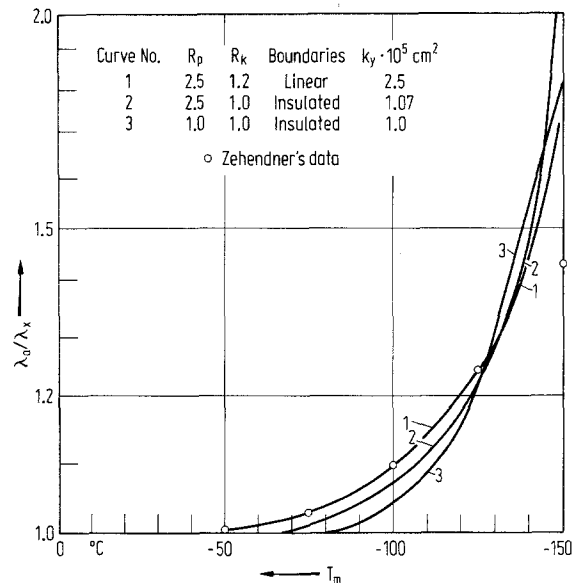

Fig. 9. Comparison with Zehendner's data (indicated by circles) for a temperature difference of 40 °C. Curve numbers 1 and 2 represent variable property solutions. Curve 3 represents the constant property solution. Property values at mean temperature are used.

in high temperature gradients and high values of (λ_{a1}/λ_x) in this region (Fig. 7). This corresponds to what has been reported by Lotz [11] and Cammerer [20].

The only experimental data with which a detailed quantitative comparison is possible is that of Zehendner. The comparison is made in Figs. 8 and 9. For this purpose λ_x was chosen to be the value of the conductivity obtained experimentally during the downward flow of heat at the same mean temperature and the same temperature gradient. Further one has to choose a value for k_y as the value for the specimen used by Zehendner is not known. This is so chosen that the theoretical value of (λ_a/λ_x) at $-100\,°C$ and $20\,°C/cm$ temperature gradient coincides with the experimentally obtained value. Three different solutions are compared with the experimental data:

1. The variable property anisotropic analysis with the temperature distribution along the horizontal faces being considered linear.

2. The variable property anisotropic analysis, with the horizontal faces being considered insulated.

3. The isotropic analysis.

For the anisotropic analysis, one also needs to know the value of R_p. Based on the results presented in Table 1, this was chosen to be 2.5 as the specimen was of superfine glass wool of density $8\,kg/m^3$. The values of k_y obtained for the three solutions with matching at $-100\,°C$ and $20\,°C/cm$ were 2.5×10^{-5}, 1.07×10^{-5} and $1.0 \times 10^{-5}\,cm^2$. These values are in order of magnitude agreement with the values expected

from the results of Table 1. It will be noted that both the anisotropic solutions are in much better agreement with the experimental data than the isotropic analysis and that the linear temperature boundary condition solution fits the data almost exactly above $-100\,°C$. This appears to be reasonable since Zehendner's experimental set-up permitted convective currents in the guard heater section. Such currents would disturb the temperature distribution at the top and bottom edges of the specimen considerably. As a result the boundary conditions would be more closely idealised by the linear variation condition.

However at temperatures below $-125\,°C$ the agreement between the analysis and the experimental results is not good. At these temperatures the Rayleigh number is high. Considerable convective flow would occur both in the main specimen as well as the guard heater section resulting in considerable deviation even from the linear temperature distribution. Furthermore, at an average temperature of $-150\,°C$ and a temperature difference of $80\,°C$, the cold face temperature is $10\,°C$ lower than the boiling point of oxygen $(93\,°K)$. Liquefaction of the gas and its effect on the apparent thermal conductivity have not been taken into account in this analysis and some deviation on this account may also be expected.

References

1. Dulnev, G. N., Komkova, L. A.: Analysis of experimental data on the heat conductivity of solid porous systems, Journal of Engineering Physics, Vol. 9 (1965) 517/519.
2. Finck, J. L.: Mechanism of heat flow in fibrous materials, Bureau of Standards, Journal of Research, Vol. 5 (1930) 974/984.
3. Hager, E., Steere, R. C.: Radiant heat transfer in fibrous thermal insulation, Journal of Applied Physics, Vol. 38 (1967) 4663/4668.
4. Van der Held, E. F. M.: The contribution of radiation to the conduction of heat, Applied Scientific Research, Vol. A III (1952) 237/249 and Vol. A IV (1954) 77/99.
5. Lander, R. M.: Gas is an important factor in the thermal conductivity of most insulating materials, Heating Piping and Airconditioning Journal, Vol. 26 (Dec. 1954) 121/126.
6. Larkin, B. K., Churchill, S. W.: Heat transfer by radiation through porous insulations, A.I.Ch.E. Journal, Vol. 5 (1959) 467/474.
7. Larkin, B. K.: A study of the rate of thermal radiation through porous insulating materials, Ph. D. thesis, University of Michigan (1957).
8. Pike, J. N.: Model for solid phase heat conduction in glass fibre pad, Jorunal of Applied Physics, Vol. 40 (1969) 899/900.
9. Tye, R. P.: Thermal conductivity, Vol. 1, Academic Press Inc. (1969).
10. Verschoor, J. D., Greebler, P.: Heat transfer by gas conduction and radiation in fibrous insulations, Trans. A.S.M.E., Vol. 74 (1952) 961/968.
11. Lotz, W. A.: Heat and air transfer in cold storage insulation, ASHRAE Transactions, Vol. 70 (1964) 181/188.
12. Wolf, S.: A theory for the effects of convective air-flow through fibrous thermal insulation, ASHRAE Transactions, Vol. 72 (1966), III.2.1/III.2.9.
13. Chan, B. K. C., Ivey, C. M., Barry, J. M.: Natural convection in enclosed porous media with rectangular boundaries, Trans. A.S.M.E., J. Heat Transfer, Vol. 92 (1970) 21/27.
14. Elder, J. W.: Steady free convection in a porous medium heated from below, Journal of Fluid Mechanics, Vol. 27 (1967) 29/48.
15. Höglund, I.: Hogisolerande ytterräggars värmemotstånd, Kungliga Tekniska Hogskolan, Stockholm (1963).
16. Allcut, E. A.: An analysis of heat transfer through thermal insulating materials, General Discussion on Heat Transfer, A.S.M.E., 11th Sept. to 13th Sept. 1951, London, 232/235.
17. Allcut, E. A., Ewens: Thermal conductivity of insulating material, Can. J. Research, Vol. A 17 (1939) 209.
18. Baker, C. K.: Effect of natural convection on apparent thermal conductivities of porous insulants, Ph. D. thesis, University of Leeds (1967).
19. Cammerer, W. F.: Die Messung der Wärmeleitfähigkeit von Isolierstoffen bei tiefen Temperaturen, Kältetechnik, Vol. 12 (1960) 107/110.
20. Cammerer, W. F.: Der Konvektionseinfluß auf die Wärmeleitfähigkeit von Wandisolierungen aus Mineralfasern, Allgemeine Wärmetechnik, Band 11, Heft 6 (1962) 95/101.
21. Griffiths: Heat insulators, Spec. Report 35, Food Investigations Board, Dept. Sci. and Ind. Research, His Majesty's Stationery Office, London (1929).
22. Katto, Y., Masuka, T.: Criterion for the onset of convective flow in porous medium, Int. J. Heat and Mass Transfer, Vol. 10 (1967) 293/309.
23. Kostelyne, V. M., Nabator, V. G.: Heat transfer in disperse insulator, Journal of Engineering Physics, Vol. 9 (1965) 377/383.
24. Wilkes, G. B.: Heat insulation, John Wiley and Sons (1950).
25. Wolf, S. et al.: Convective air-flow effects with mineral wool insulation in wood frame walls, ASHRAE, Transactions, Vol. 72 (1966) III.3.1/III.3.8.
26. Zehendner, H.: Einfluß der freien Konvektion auf die Wärmeleitfähigkeit einer leichten Mineralfasermatte bei tiefen Temperaturen, Kältetechnik, Vol. 16 (1964) 308/311.
27. Gill, A. E.: A proof that convection in a porous vertical slab is stable, Journal of Fluid Mechanics, Vol. 35 (1969) 545/547.
28. Rubel, A., Landis, F.: Numerical study of natural convection in a vertical rectangular enclosure, The Physics of Fluids, Vol. 12 (1969) II 209/213.

Research Scholar D. K. Joshi
Prof. Dr. S. P. Sukhatme
Department of Mechanical Engineering
Indian Institute of Technology
Powai, Bombay 76 (India)